Molecular-level Insights on Reactive Arrangement in On-surface Photocatalytic Coupling Reactions using Tip-enhanced Raman Spectroscopy

Zhen-Feng Cai[1], Juan Pedro Merino[2], Wei Fang[1,3], Naresh Kumar[1]*, Jeremy O. Richardson[1], Steven De Feyter[2] and Renato Zenobi[1]*

[1]Department of Chemistry and Applied Biosciences, ETH Zurich, Vladimir-Prelog-Weg 3, Zurich CH-8093, Switzerland

[2]Department of Chemistry, Division of Molecular Imaging and Photonics, KU Leuven, Celestijnenlaan 200F, B-3001 Leuven, Belgium

[3]Department of Chemistry, Fudan University, Shanghai 200438, P. R. China

ABSTRACT: Plasmon-enhanced photocatalytic coupling reactions have been used as model systems in surface-enhanced Raman spectroscopy and tip-enhanced Raman spectroscopy (TERS) research for decades. However, the role of reactive arrangement on efficiency of these model reactions has remained largely unknown to date often leading to conflicting interpretations of experimental results. Herein, we use an interdisciplinary toolbox of nanoscale TERS imaging in combination with molecular-resolution ambient scanning tunnelling microscopy (STM) and density functional theory (DFT) modelling to investigate the role of reactive arrangement in photocatalytic coupling of 4-nitrobenzenethiol (4-NTP) to p,p'-dimercaptoazobisbenzene (DMAB) on single-crystal and polycrystalline Au surfaces for the first time. TERS imaging with 3 nm resolution clearly revealed a significantly higher catalytic efficiency inside a kinetically-driven disordered phase of the 4-NTP adlayer compared to the thermodynamically stable ordered phase on Au. Furthermore, molecular level details of the self-assembly structures in the disordered and ordered phases obtained using ambient high-resolution STM enabled an unambiguous structure-reactivity correlation of photocatalytic coupling. Finally, quantitative mechanistic insights obtained from DFT modelling based on the accurate parameters determined from STM imaging, emphatically confirmed that a combination of steric hindrance effect and energetic barrier leads to a lower reaction efficiency in the ordered phase of 4-NTP adlayer. This fundamental study establishes the first direct structure-reactivity correlation in on-surface photocatalytic coupling reactions and highlights the critical role of reactive arrangement in the efficiency of on-surface coupling reactions in heterogeneous catalysis.

INTRODUCTION

Plasmon-enhanced photocatalytic reactions have attracted immense attention in recent years because of their novel applications in H_2 dissociation,[1] CO_2 to fuel conversion,[2] water splitting,[3] ammonia synthesis[4] and catalytic oxidation reactions including ethylene epoxidation and CO and NH_3 oxidation.[5] Amongst these, photocatalytic coupling of 4-nitrothiophenol (4-NTP) and 4-aminothiophenol (4-ATP) to p,p'-dimercaptoazobenzene (DMAB) has served as a model reaction system in surface-enhanced Raman spectroscopy (SERS)[6] and tip-enhanced Raman spectroscopy (TERS)[7-10] research for decades. The efficiency of the plasmon-enhanced photocatalytic coupling reactions has been found to be strongly influenced by temperature,[11] excitation laser parameters,[12, 13] substrate[14, 15] and the surrounding environment.[16-17] In addition to these, since all reaction steps in the photocatalytic coupling of 4-NTP → DMAB and 4-ATP → DMAB are surface-confined, specific reactive arrangement of the adsorbed reactant molecules on a catalyst surface is also expected to critically influence efficiency. However, the role of the reactive arrangement (orientation and surface coverage of the reactive species) of adsorbed molecular species on reaction efficiency has remained entirely unclear to date, primarily due to the difficulty in monitoring interfacial catalytic reactions with ultra-high sensitivity and molecular-resolution under ambient conditions. Furthermore, this fundamental lack of structure-reactivity understanding often leads to conflicting reports on plasmon-driven photocatalytic coupling reactions in literature.[18-19]

Surface-sensitive analytical tools capable of *operando* tracking of interfacial catalytic processes are of prime importance for determining structure-reactivity relationships.[20-21] For example, correlative scanning tunnelling microscopy (STM)-based topography and X-ray photoelectron spectroscopy (XPS)-based chemical analysis are the commonly used tools for investigating on-surface coupling reactions.[22] However, the microscale spatial resolution of XPS precludes analysis of reactive arrangement at nanometer length-scales and a direct correlation with molecular-resolution STM images is not possible. On the other hand, infra-red and Raman spectroscopies are widely used techniques for *in-situ* characterization of catalytic reactions, nevertheless they suffer from the limitations of low sensitivity and spatial resolution.[23-24] For catalytic interfaces on rough plasmonic substrates, SERS can yield valuable chemical information with a single molecule sensitivity. Still, the lateral resolution remains diffraction-limited to the sub-micron scale and large spatial variation of signal enhancement prevents reliable investigation of on-surface reactive arrangement.[25-26]

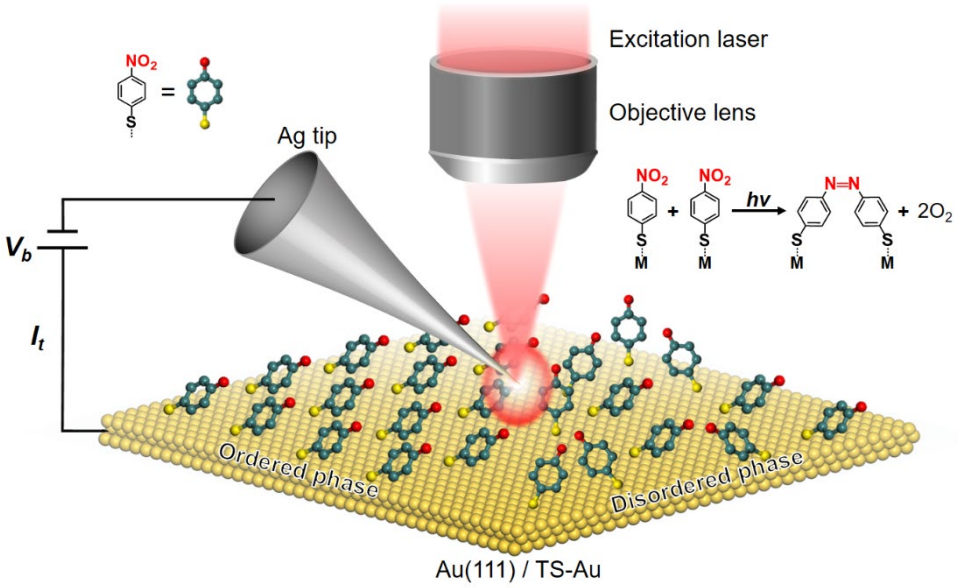

Figure 1. Schematic diagram of the STM-TERS set-up used in this study to investigate reactive arrangement in photocatalytic coupling of 4-NTP → DMAB on polycrystalline and single-crystal Au surfaces.

Over the last two decades, TERS has emerged as a powerful nanoanalytical tool for surface chemical imaging with a nanoscale spatial resolution under ambient conditions.[27-28] The ultrahigh sensitivity and spatial resolution have made it a promising tool for tracking on-surface catalytic reactions.[29-30] For example, van Schrojenstein Lantman *et al.* utilized the catalytic activity of Ag-coated TERS probes under green laser irradiation to trigger and with red laser irradiation to monitor photocatalytic conversion of 4-NTP → DMAB over time.[31] Van Duyne and collaborators utilized TERS to investigate the metallophthalocyanines-catalyzed oxygen reduction reaction on single crystal electrodes to capture reactive intermediates and products.[32-33] More recently, Sun *et al.* attempted to investigate the effect of adsorption orientation on photocatalytic conversion of 4-NTP and 4-ATP → DMAB on single crystal Ag and Au substrates using TERS.[19] However, this study lacked spatially-resolved visualization of product formation as well as high-resolution imaging of molecular arrangement. Consequently, a clear correlation of reactive arrangement with reaction efficiency could not be established. To the best of our knowledge, none of the TERS or SERS studies to date has established a clear structure-reactivity relationship for the nanoscale arrangement of reactive species on a mono- or polycrystalline catalyst surface.

Herein, using an interdisciplinary combination of high-resolution TERS imaging, ambient molecular-resolution STM and density functional theory (DFT) modelling, we present a comprehensive investigation of the reactive arrangement of 4-NTP on polycrystalline Au and single-crystal Au(111) surfaces to establish structure-reactivity relationships in the local environment. TERS imaging of the 4-NTP → DMAB plasmon-enhanced coupling reveals a clear difference in the reaction efficiency in a kinetically-driven disordered phase compared to the thermodynamically stable ordered phase. TERS results are supported with molecular-level details of the self-assembly structures of the disordered and ordered phases obtained using ambient molecular-resolution STM imaging. Finally, DFT modelling set up using the accurate parameters determined from STM imaging, provides novel mechanistic insights revealing steric hindrance effects, which lead to a lower reaction efficiency in the ordered phase of 4-NTP adlayer. This fundamental work paves the way for optimizing efficiency of photocatalytic as well as other on-surface coupling reactions for fabrication of novel functional materials including organic macromolecules, two-dimensional (2D) organic networks, graphene nanoribbons and super honeycomb networks through correlative high-resolution TERS imaging, molecular-resolution STM and DFT modelling.

RESULTS AND DISCUSSION

A schematic diagram of the STM-TERS set-up used is shown in Figure 1. It is well-established that 4-NTP molecules adsorbed on plasmonic surfaces *via* self-assembly can be activated and converted into an azo species, DMAB,[31,34] which can be easily monitored using its Raman signature. Therefore, the 4-NTP → DMAB plasmon-enhanced coupling reaction was employed as the model reactive system in this study. The spatial arrangement of 4-NTP molecules on the catalyst surface was controlled by taking advantage of the time-dependent self-assembly process of the thiolate molecules.[35-36] Disordered and well-ordered phases of the 4-NTP self-assembled monolayer (SAM) are constructed *via* drop-cast and immersion protocols, respectively, as described in the Experimental Details presented in the Supporting Information. In addition, Au(111) and template-stripped Au (TS-Au) substrates were applied as model single-crystal and polycrystalline platforms to investigate the coupling reaction on substrates with different surface roughness (see Figure S1 for details).

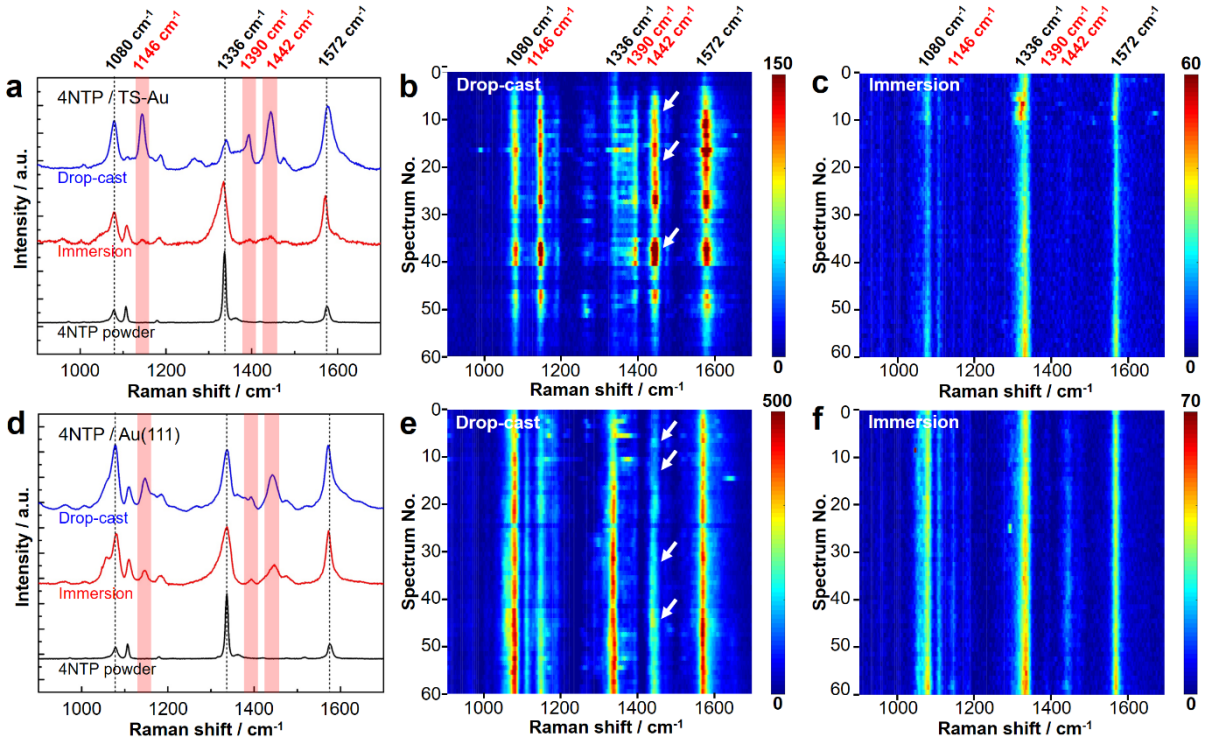

Figure 2. TERS spectra of 4-NTP functionalized (a) TS-Au and (d) Au(111) surfaces prepared *via* drop-cast (blue trace) or immersion (red trace) protocols. Each spectrum represents an average of 60 TERS spectra measured in an area of 0.6 μm^2 with a step size of 100 nm. The Raman spectrum of 4-NTP powder (black trace) is also plotted for comparison. Characteristic DMAB peaks at 1146, 1390, and 1442 cm^{-1} are highlighted in red. Waterfall plots of the spectra measured in the TERS images of a 4-NTP SAM on (b, c) TS-Au and (e, f) Au(111) surfaces prepared *via* drop-cast and immersion methods. In (b) and (e), spatial variation in formation of DMAB on the drop-cast samples is highlighted with arrows. All TERS measurements in (a) – (f) were performed using the same Ag tip.

Figure 2a shows the averaged TERS spectra of 4-NTP adlayers on polycrystalline TS-Au surfaces prepared *via* drop-cast and immersion methods. The averaged TERS spectrum measured on TS-Au appear different from the powder Raman spectrum of 4-NTP (black trace in Figure 2a) due to the photocatalytic conversion of 4-NTP → DMAB. In addition to the characteristic Raman bands of 4-NTP (labelled by black dashed lines), three new bands of the DMAB product (highlighted by red stripes) appear in the TERS spectra at 1146 cm^{-1} (ν_{C-N}), 1390 cm^{-1} ($\nu_{N=N}$), and 1442 cm^{-1} ($\nu_{N=N}$).[19,37-38]. Interestingly, the TERS signal intensity of the three DMAB peaks from the drop-cast sample differs significantly from the immersion sample. The intensity ratio between the 1442 cm^{-1} peak to the 1080 cm^{-1} peak (I_{1442}/I_{1080}) is a measure of product formation in 4-NTP → DMAB reaction.[9] I_{1442}/I_{1080} ratio is found to be 1.2 for the drop-cast sample, whereas it is only 0.3 for the immersion sample, which indicates a significantly higher reaction efficiency on the drop-cast sample. To further visualize the spectral differences, spectra measured in the TERS images are displayed as waterfall plots in Figures 2b and 2c. In these plots, a significantly higher intensity DMAB bands (1146, 1390 and 1442 cm^{-1}) are observed on the drop-cast sample. Furthermore, a highly non-uniform distribution of DMAB intensity is seen at different locations of the drop-cast sample. On the other hand, the intensity of the DMAB bands is much weaker on the immersion sample, whilst the intensity distribution stays largely constant. This indicates that the reactivity of 4-NTP adlayers in the drop-cast sample is relatively much higher and varies significantly across the sample surface, whilst the reactivity is lower on the immersion sample and remains largely uniform throughout the surface.

In order to further investigate the observed difference in reactivity of drop-cast and immersion samples, an atomically flat Au(111) substrate was applied as a single-crystal platform to investigate the on-surface photocatalytic coupling reaction. Figure 2d displays the averaged spectra of TERS images of 4-NTP adlayer on Au(111) prepared *via* drop-cast and immersion methods. Similar to the TS-Au surface, a significantly higher reactivity is observed on the drop-cast sample (I_{1442}/I_{1080} = 0.6) compared to the immersion sample (I_{1442}/I_{1080} = 0.3). The spectral differences in the TERS images are also displayed as waterfall plots in Figures 2e and 2f. Interestingly, on the drop-cast sample, the reactivity of 4-NTP → DMAB is relatively lower on Au(111) compared to TS-Au (Figure 2a). We propose that this is because of the irregular orientation of 4-NTP molecules on the rough TS-Au surface, which provides them a greater chance to adopt favorable configurations for reactive coupling as discussed later.

Notably, we also observed very similar spectral and reactivity differences in a slightly different but related on-surface photocatalytic coupling reaction, namely, the oxidative

dimerization of 4-ATP → DMAB on TS-Au and Au(111) prepared *via* drop-cast and immersion protocols. These results are presented in Figure S2. A significantly higher amount of DMAB was observed on the drop-cast samples (I_{1442}/I_{1080} = 0.7 on TS-Au and 0.8 on Au(111)) compared to the immersion samples (I_{1442}/I_{1080} = 0.2 on TS-Au and 0.3 on Au(111)). Considering all TERS measurements for a particular reactant (4-NTP or 4-ATP) on different Au surfaces were performed using the same probe and under the same experimental conditions (laser wavelength, laser power, temperature, etc.), the decisively different reactivity of the drop-cast and immersion samples strongly points towards a significantly different reactive arrangement.

To test our hypothesis and establish a clear structure-reactivity relationship, high-resolution STM imaging was carried out to visualize molecular-level details of the self-assembly structures on Au(111) surface constructed using drop-cast and immersion protocols. STM images of the 4-NTP monolayer on Au(111) formed through the immersion method are presented in Figures 3a and S3, where most of the surface is found to be uniformly covered by well-ordered molecular arrays. Additionally, some fuzzy features are observed in a few areas of the images. Since 4-NTP molecules adsorb on Au *via* strong S-Au covalent interaction, the fuzzy features in the image are ascribed to the 4-NTP molecules with irregular orientation. Such molecules are not fixed rigidly by close packing with their neighbors but have the freedom to rotate around the S-Au bond at least partially. The size of the well-ordered 4-NTP domains varies from 25 - 441 nm^2 with a surface coverage of 74.3% ± 5.5%. High-resolution STM images showing the packing details of the 4-NTP molecules on Au(111) surface are presented in Figures 3b and S4. Each 4-NTP molecule appears as a bright spot in the image and such bright spots form a well-ordered close-packed structure. From the high-resolution images, average distance between two adjacent 4-NTP molecules is estimated to be 0.8 ± 0.1 nm (Figures 3c and S4).

In contrast, STM images of the drop-cast sample in Figures 3d and S5 show only a few small areas (6~30 nm^2) of close-packed 4-NTP domains on the Au(111) surface with a coverage of only 7.8% ± 1.0% indicating that most of the sample surface is covered by molecules with irregular orientation. In the ordered domains, the intermolecular distance is estimated from the high-resolution STM images in Figures 3e, 3f and S6 to be 0.8 ± 0.1 nm, which is very similar to the immersion sample. Figure 3g shows a molecularly resolved STM image of the close-packed phase, in which each 4-NTP molecule is visible as an oval-shaped bright spot. The length of each spot is *ca.* 0.7 nm (see Figures 3h and 3i) and a small height variation is observed inside single spots as highlighted by yellow arrows in Figure 3g. Since the DFT calculated length of a 4-NTP molecule is *ca.* 0.72 nm (illustrated in Figure S7), this indicates that 4-NTP molecules inside the well-ordered domains are adsorbed with a large tilt angle away from the surface normal, i.e. they lie almost flat on the surface. Correlation of TERS results in Figure 2 with the structural difference in molecular packing of immersion and drop-cast samples suggests that the well-ordered close-packed arrangement of 4-NTP molecules is in fact unfavorable to the efficiency of on-surface 4-NTP → DMAB photocatalytic coupling reaction.

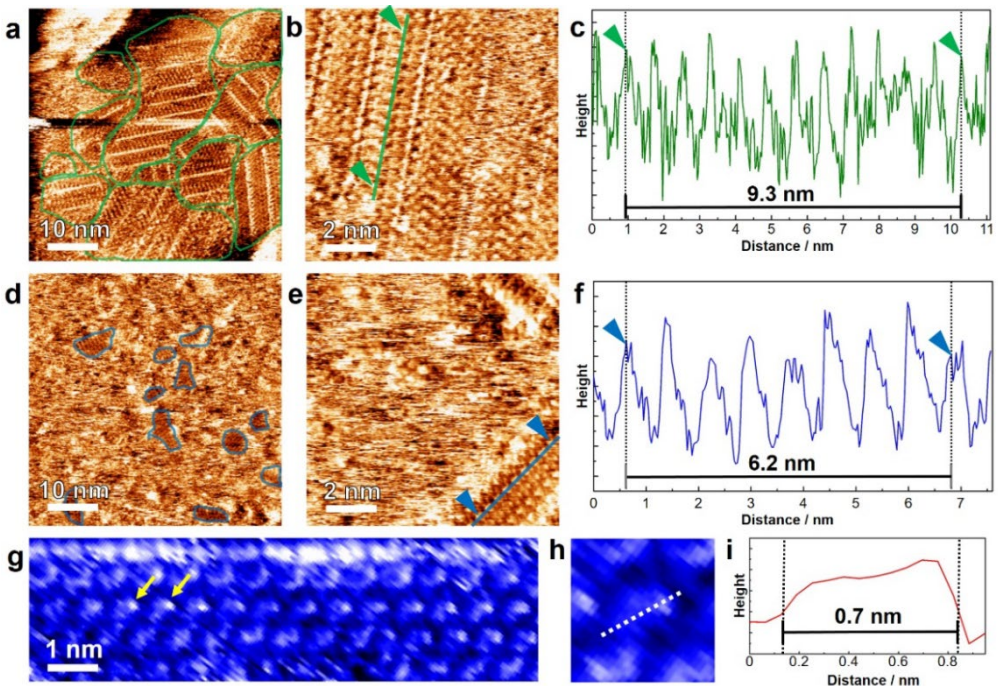

Figure 3. (a), (b) High-resolution STM images of the 4-NTP adlayer at the air/Au(111) interface prepared *via* the immersion protocol. (c) Height profile along the line marked in (b). (d), (e) High-resolution STM images of the 4-NTP adlayer at the air/Au(111) interface prepared *via* drop-cast protocol. (f) Height profile along the line marked in (e). STM parameters in (a) and (b): I_t = 0.11 nA; V_{bias} = –0.20 V, and in (d) and (e): I_t = 0.15 nA; V_{bias} = –0.20 V. (g) Single-molecule resolved STM image of 4-NTP molecules inside a well-ordered domain. Scale bar: 1 nm. (h) STM image of a single 4-NTP molecule. (i) Height profile along the dashed line marked in (h).

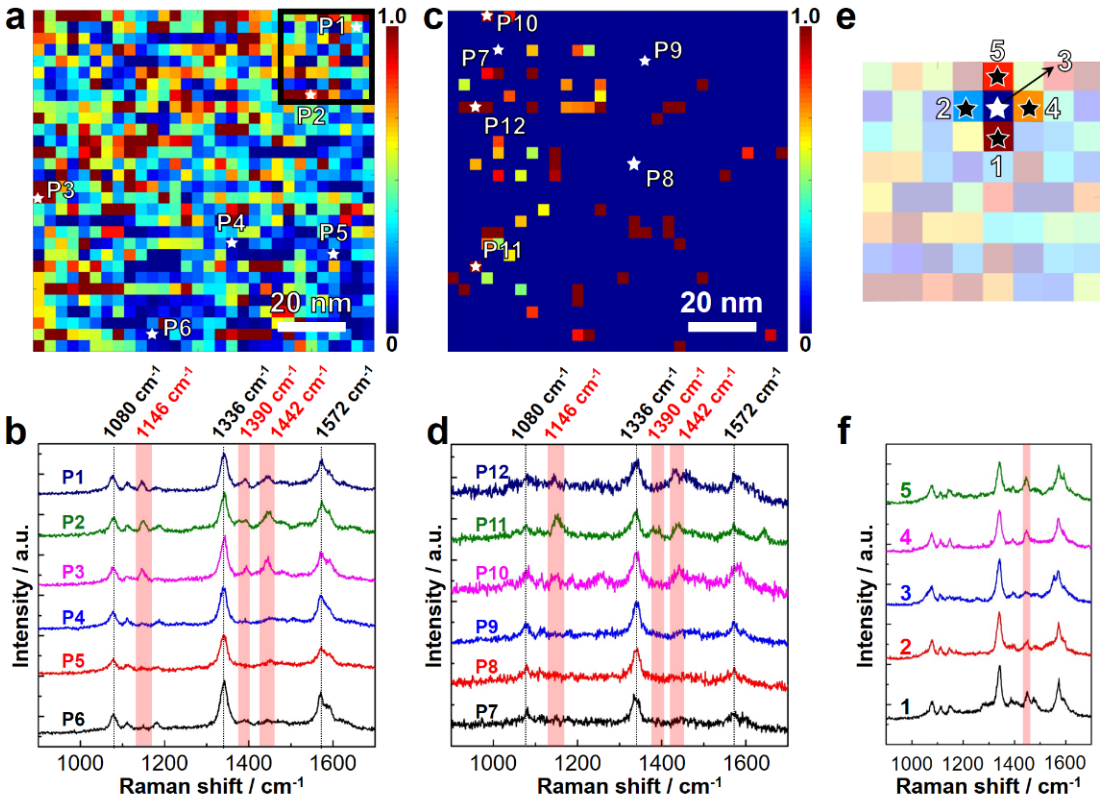

Figure 4. High-resolution TERS images of I_{1442}/I_{1080} ratio measured on samples prepared *via* (a) drop-cast and (c) immersion protocols on single-crystal Au(111) surfaces. Step size: 3.3 nm. Spectrum integration time: 1 s. (b), (d) TERS spectra measured at the locations P1-P12 marked in (a) and (c). (e) Zoomed-in TERS image of the region marked in (a). Five pixels labelled as 1-5 are highlighted. (f) TERS spectra measured at the pixels labelled in (e).

To directly visualize the effect of molecular arrangement on reaction efficiency, we performed high-resolution 2D TERS imaging of the 4-NTP → DMAB reaction *in situ* on both Au(111) and TS-Au surfaces. High-resolution TERS images of the I_{1442}/I_{1080} ratio measured on the drop-cast and immersion samples on Au(111) are shown in Figure 4. Most of the drop-cast sample surface is found to be covered with DMAB product (Figure 4a) along with some unreacted 4-NTP. Six selected TERS spectra from locations of DMAB formation (P1-P3) and unreacted 4-NTP (P4-P6) plotted in Figure 4b confirm this observation. DMAB bands are observed only at P1-P3 signifying that the photocatalytic coupling only occurs at these locations. In contrast, most of the immersion sample surface shows no product formation (Figure 4c) and the reaction occurs in only a few small, isolated regions. This can be seen clearly in the selected TERS spectra plotted in Figure 4d where DMAB formation is observed only at locations P9-P12. A zoomed-in TERS image of the region marked in Figure 4a is shown in Figure 4e, where five pixels (1-5) are highlighted. TERS spectra from these pixels are plotted in Figure 4f, which show that DMAB product is formed at all positions except 3. Since the step size of TERS imaging is 3.3 nm, this indicates a spatial resolution of *ca.* 3 nm. The surface coverage of the DMAB product formation on the drop-cast and immersion samples in (a) and (b) is estimated to be *ca.* 72.3% and 7.2%, respectively. Interestingly, this correlates inversely with the surface coverage of the well-ordered domains on drop-cast (7.8%) and immersion samples (74.3%) thereby strongly supporting our hypothesis that a close-packed molecular arrangement is inefficient for the 4-NTP → DMAB reaction.

Noticeably, similar results are obtained in the high-resolution TERS imaging of the 4-NTP → DMAB reaction on polycrystalline TS-Au surface, which is presented in Figure 5. Once again, a significantly higher level of DMAB product is observed on the drop-cast sample compared to the immersion sample. Furthermore, surface coverage of product formation on the drop-cast sample is found to be significantly higher (*ca.* 82.0%, Figures 5a) than the immersion sample (*ca.* 18.2 %, Figures 5c) indicating that a close-packed molecular arrangement prevents efficient photocatalytic coupling of 4-NTP → DMAB on both single-crystal and polycrystalline Au surfaces.

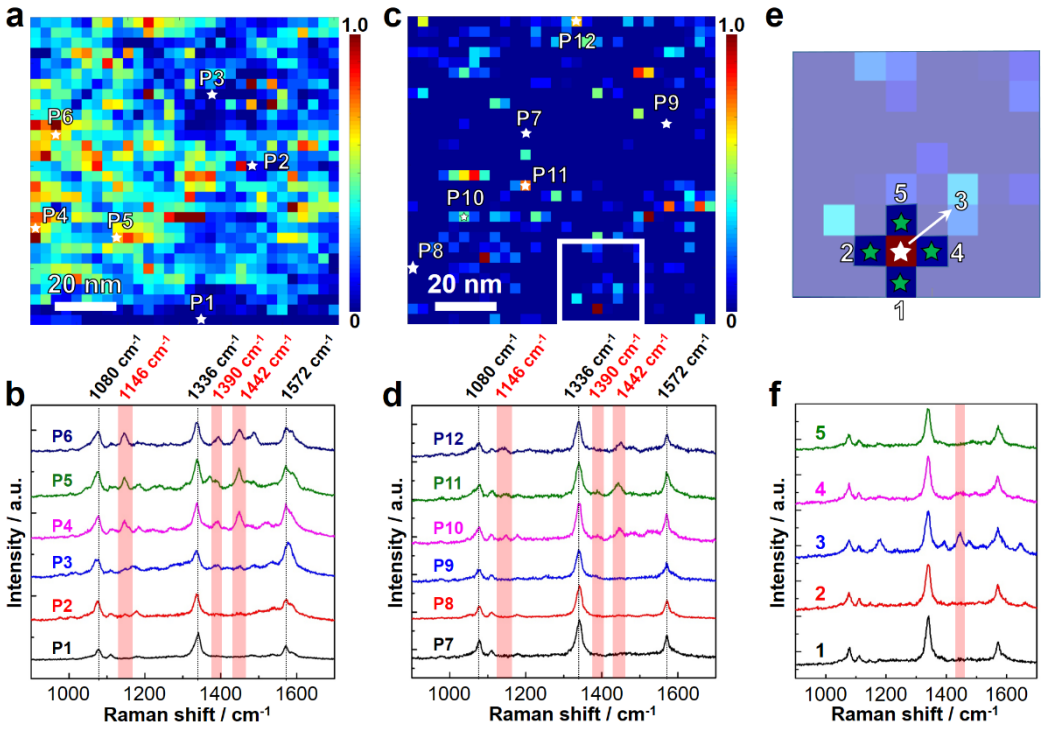

Figure 5. High-resolution TERS images of I_{1442}/I_{1080} ratio measured on samples prepared *via* (a) drop-cast and (c) immersion protocols on polycrystalline TS-Au surfaces. Step size: 3.3 nm. Spectrum integration time: 1 s. (b), (d) TERS spectra measured at the locations P1-P12 marked in (a) and (c). (e) Zoomed-in TERS image of the region marked in (c). Five pixels labelled as 1-5 are highlighted. (f) TERS spectra measured at the pixels labelled in (e).

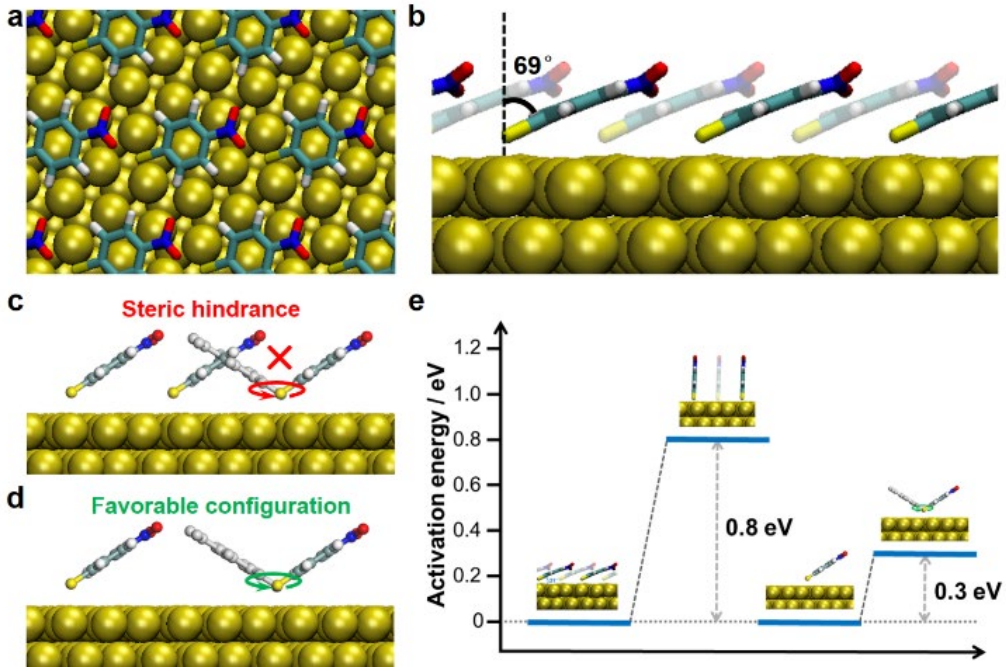

Figure 6. (a) Top and (b) side views of the optimal close-packed 4-NTP adlayer structure on Au(111) calculated using DFT. The atoms are colored as follows: H, white; C, cyan; S, yellow; N, dark blue; O, red; Au, gold. In (b), the dark and light-colored molecules represent the front and back rows, respectively. Schematic diagrams illustrating (c) steric hindrance between two adjacent molecules inside the close-packed phase of 4-NTP adlayer and (d) favorable configuration for the photocatalytic coupling of 4-NTP → DMAB inside the disordered phase. (e) Plot depicting calculated activation energy barriers for change of orientation from a flat-lying to an upright geometry in the closed-packed phase and rotation of a 4-NTP molecule in the disordered phase.

To gain mechanistic insights into the relationship of reactive arrangement with reaction efficiency, we performed DFT simulations of the optimal adsorption configuration of a 4-NTP close-packed monolayer on Au(111) surface. Unlike previous reports[19], these DFT simulations were based on the accurate intermolecular distance and surface coverage parameters determined from the high-resolution STM images. Figure 6a and 6b show the top and side views of the optimal structure of the close-packed 4-NTP adlayer. In agreement with the STM results (Figures 3g-3i), the DFT calculated 4-NTP structures confirm a large tilt angle of 69° in the close-packed phase (Figure 6b). Notably, this tilt angle is significantly higher than previously report,[19] and slightly lower than the adsorption angle of 4-mercaptobenzonitrile reported by El-Khoury *et al.*[39] However, unlike our study, none of the previous DFT simulation models were based on the empirically determined parameters.

Under ambient conditions, the reductive coupling of 4-NTP → DMAB is catalyzed by plasmonically activated atomic hydrogen *via* two possible pathways:[40] (1) both oxygen atoms of a 4-NTP molecule are removed through formation of an N−HO−Au transition state followed by the azo coupling with a similarly deoxygenated adjacent molecule. (2) A single oxygen atom is removed from two adjacent 4-NTP molecules first, which then undergo azo coupling with the subsequent removal of two remaining oxygen atoms. Both reaction mechanisms require nitrogen atoms on adjacent 4-NTP molecules to come in contact for azo bond formation. However, this is not feasible in the well-ordered phase of the 4-NTP adlayer. In close-packed arrangement, 4-NTP molecules cannot adopt the configuration required for azo coupling *via* rotation, due to steric hindrance as schematically illustrated in Figure 6c. Additionally, nitrogen atom contact *via* an alternative mechanism, i.e. 4-NTP "standing up", is energetically unfavorable. The upright adsorption geometry of 4-NTP molecule is ~0.8 eV less stable than the almost flat-lying geometry as depicted in Figure 6e, which corresponds to an equilibrium constant on the order of 10^{-13} at room temperature.

Therefore, we propose that the low efficiency of 4-NTP → DMAB coupling reaction in the close-packed phase of the immersion samples arises from the inability of 4-NTP molecules to adopt a spatially favorable configuration due to a combination of steric hindrance and an energetic barrier. In contrast, when 4-NTP molecules are not closely packed, they can rotate quite easily on the surface since they only need to overcome a small energy barrier of ~0.3 eV as shown in the DFT simulation results in Figure S8 and illustrated in Figures 6d and 6e. Assuming an attempt frequency on the order of fs, the rate constant for a 4-NTP rotation is on the order of ns. Therefore, in the disordered phase of the drop-cast samples, the irregularly oriented 4-NTP molecules have a much higher chance to adopt favorable configurations for efficient photocatalytic transformation of 4-NTP → DMAB.

This correlation of reactive arrangement with reaction efficiency provides a cogent mechanistic explanation of the high-resolution TERS results shown in Figures 4 and 5, where more than 72.3% of the drop-cast sample surface is covered with DMAB product molecules. In contrast, less than 18.2% of the immersion sample surface shows DMAB formation, which mostly contains well-ordered domains of the close-packed 4-NTP adlayer as revealed by high-resolution STM imaging.

An attempt was also made to study reactions kinetics on the drop-cast and immersion samples, but the photocatalytic conversion of 4NTP → DMAB was found to occur instantly on both samples on the timescale of our measurements. Therefore, time-dependent information about reactant to product conversion for investigation of reaction kinetics could not be obtained unlike in a previous SERS study reported by van Schrojenstein Lantman *et al.*, where time-dependent conversion of 4-NTP to DMAB could be monitored using very low excitation laser power density provided by a 5x, 0.12 NA objective lens.[41] Whilst it is easier to perform time-resolved studies using SERS due to the presence of a large number of SERS hotspots in the probed area that can provide good quality spectra even at a very low laser power, this is generally not possible in TERS due to the existence of only one hotspot between the metallic TERS probe and the sample. The biggest strength of TERS lies in spatially resolved molecular analysis, which is the focus of our current work.

CONCLUSIONS

In summary, we have applied correlative high-resolution TERS imaging combined with ambient molecular-resolution STM and DFT simulations to investigate the effect of reactive arrangement on photocatalytic coupling of 4-NTP → DMAB on single-crystal Au(111) and polycrystalline TS-Au surfaces to establish clear structure-reactivity relationships in the local environment. TERS imaging of the plasmon-enhanced coupling reaction clearly showed a higher efficiency in a kinetically-driven disordered phase compared to the thermodynamically stable ordered phase. Furthermore, molecular level details of the self-assembly structures of the disordered and ordered phases of 4-NTP adlayer on Au(111) obtained using high-resolution ambient STM imaging enabled a direct correlation of molecular arrangement with reaction efficiency. Finally, structure-reactivity mechanistic insights obtained using DFT simulations confirmed that a combination of steric hindrance effect and energetic barrier clearly favors a higher reaction efficiency in the disordered phase compared to a well-packed ordered phase. These fundamental insights also provide a possible explanation for the conflicting results reported in the SERS and TERS literature on model plasmon-enhanced photocatalytic coupling reactions, where a low reaction efficiency resulting from a close-packed molecular arrangement could be misinterpreted as a lack of plasmonic signal enhancement. Therefore, the clear structure-reactivity relationship in on-surface photocatalytic coupling reactions established in this work is expected to facilitate a rational experimental design as well as better data interpretation in the future SERS and TERS studies. Furthermore, the novel structure-reactivity insights deciphered in this fundamental study highlight the critical role of reactive arrangement in on-surface heterogeneous catalytic reactions at large.

ASSOCIATED CONTENT

Supporting Information. The Supporting Information is available free of charge at http://pubs.acs.org.

Contents: Experimental section; STM images of Au(111) and TS-Au; Averaged TERS spectra and waterfalls of 4-ATP/Au(111) and 4-ATP/TS-Au; High-resolution STM images of 4-NTP/Au(111); DFT optimized structural models of 4-NTP; Activation energy required for 4-NTP to rotate on Au(111).

AUTHOR INFORMATION

Corresponding Author

* kumar@org.chem.ethz.ch; zenobi@org.chem.ethz.ch

Notes

The authors declare no competing financial interest.

The original data used in this publication are made available in a curated data archive at ETH Zurich (https://www.researchcollection. ethz.ch) at https://doi.org/10.3929/ethz-b-000500731

ACKNOWLEDGMENT

The High Performance Computing Team at ETH Zurich is thanked for providing technical support for DFT calculations. ZFC, NK and RZ acknowledge funding from the ERC program (Grant No. 741431− 2DNanoSpec). SDF and JPM acknowledge KU Leuven internal funds (Grant No. C14/19/079) and the Research Foundation Flanders (FWO) for financial support.

REFERENCES

(1) Mukherjee, S.; Libisch, F.; Large, N.; Neumann, O.; Brown, L. V.; Cheng, J.; Lassiter, J. B.; Carter, E. A.; Nordlander, P.; Halas, N. J. Hot Electrons Do the Impossible: Plasmon-Induced Dissociation of H2 on Au. *Nano Lett.* **2013**, *13*, 240.

(2) Yu, S.; Wilson, A. J.; Kumari, G.; Zhang, X.; Jain, P. K. Opportunities and Challenges of Solar-Energy-Driven Carbon Dioxide to Fuel Conversion with Plasmonic Catalysts. *ACS Energy Lett.* **2017**, *2*, 2058.

(3) Ingram, D. B.; Linic, S. Water Splitting on Composite Plasmonic-Metal/Semiconductor Photoelectrodes: Evidence for Selective Plasmon-Induced Formation of Charge Carriers near the Semiconductor Surface. *J. Am. Chem. Soc.* **2011**, *133*, 5202.

(4) Oshikiri, T.; Ueno, K.; Misawa, H. Plasmon-Induced Ammonia Synthesis through Nitrogen Photofixation with Visible Light Irradiation. *Angew. Chem. Int. Ed.* **2014**, *53*, 9802.

(5) Christopher, P.; Xin, H.; Linic, S. Visible-light-enhanced catalytic oxidation reactions on plasmonic silver nanostructures. *Nat. Chem.* **2011**, *3*, 467.

(6) Sun, M.; Xu, H. A Novel Application of Plasmonics: Plasmon-Driven Surface-Catalyzed Reactions. *Small* **2012**, *8*, 2777.

(7) Hartman, T.; Wondergem, C. S.; Kumar, N.; van den Berg, A.; Weckhuysen, B. M. Surface- and Tip-Enhanced Raman Spectroscopy in Catalysis. *J. Phys. Chem. L* **2016**, *7*, 1570.

(8) Bhattarai, A.; El-Khoury, P. Z. Nanoscale Chemical Reaction Imaging at the Solid–Liquid Interface via TERS. *J. Phys. Chem. L* **2019**, *10*, 2817.

(9) Kumar, N.; Wondergem, C. S.; Wain, A. J.; Weckhuysen, B. M. In Situ Nanoscale Investigation of Catalytic Reactions in the Liquid Phase Using Zirconia-Protected Tip-Enhanced Raman Spectroscopy Probes. *J. Phys. Chem. L* **2019**, *10*, 1669.

(10) Wang, C.-F.; O'Callahan, B. T.; Kurouski, D.; Krayev, A.; El-Khoury, P. Z. The Prevalence of Anions at Plasmonic Nanojunctions: A Closer Look at p-Nitrothiophenol. *J. Phys. Chem. L* **2020**, *11*, 3809.

(11) Canpean, V.; Astilean, S. Temperature effect on the SERS signature of p-aminothiophenol: A new evidence for the production of p,p'-dimercaptoazobenzene on metallic nanostructures. *Spectrochim. Acta, Part A* **2012**, *96*, 862.

(12) Ye, J.; Hutchison, J. A.; Uji-i, H.; Hofkens, J.; Lagae, L.; Maes, G.; Borghs, G.; Van Dorpe, P. Excitation wavelength dependent surface enhanced Raman scattering of 4-aminothiophenol on gold nanorings. *Nanoscale* **2012**, *4*, 1606.

(13) Tan, E.; Yin, P.; Yu, C.; Yu, G.; Zhao, C. The oxidant and laser power-dependent plasmon-driven surface photocatalysis reaction of p-aminothiophenol dimerizing into p,p′-dimercaptoazobenzene on Au nanoparticles. *Spectrochim. Acta, Part A* **2016**, *166*, 15.

(14) Jing, H.; Zhang, Q.; Large, N.; Yu, C.; Blom, D. A.; Nordlander, P.; Wang, H. Tunable Plasmonic Nanoparticles with Catalytically Active High-Index Facets. *Nano Lett.* **2014**, *14*, 3674.

(15) Kafle, B.; Poveda, M.; Habteyes, T. G. Surface Ligand-Mediated Plasmon-Driven Photochemical Reactions. *J. Phys. Chem. L* **2017**, *8*, 890.

(16) Sun, M.; Huang, Y.; Xia, L.; Chen, X.; Xu, H. The pH-Controlled Plasmon-Assisted Surface Photocatalysis Reaction of 4-Aminothiophenol to p,p′-Dimercaptoazobenzene on Au, Ag, and Cu Colloids. *J. Phys. Chem. C* **2011**, *115*, 9629.

(17) Huang, Y.-F.; Zhang, M.; Zhao, L.-B.; Feng, J.-M.; Wu, D.-Y.; Ren, B.; Tian, Z.-Q. Activation of Oxygen on Gold and Silver Nanoparticles Assisted by Surface Plasmon Resonances. *Angew. Chem. Int. Ed.* **2014**, *53*, 2353.

(18) Zeng, Z.; Qi, X.; Li, X.; Zhang, L.; Wang, P.; Fang, Y. Nano-scale image rendering via surface plasmon-driven reaction controlled by tip-enhanced Raman spectroscopy. *Appl. Surf. Sci.* **2019**, *480*, 497.

(19) Sun, J.-J.; Su, H.-S.; Yue, H.-L.; Huang, S.-C.; Huang, T.-X.; Hu, S.; Sartin, M. M.; Cheng, J.; Ren, B. Role of Adsorption Orientation in Surface Plasmon-Driven Coupling Reactions Studied by Tip-Enhanced Raman Spectroscopy. *J. Phys. Chem. L* **2019**, *10*, 2306.

(20) Zhang, H.; Duan, S.; Radjenovic, P. M.; Tian, Z.-Q.; Li, J.-F. Core–Shell Nanostructure-Enhanced Raman Spectroscopy for Surface Catalysis. *Acc. Chem. Res.* **2020**, *53*, 729.

(21) Tao, F.; Crozier, P. A. Atomic-Scale Observations of Catalyst Structures under Reaction Conditions and during Catalysis. *Chem. Rev.* **2016**, *116*, 3487.

(22) Dong, L.; Liu, P. N.; Lin, N. Surface-Activated Coupling Reactions Confined on a Surface. *Acc. Chem. Res.* **2015**, *48*, 2765.

(23) Hess, C. New advances in using Raman spectroscopy for the characterization of catalysts and catalytic reactions. *Chem. Soc. Rev.* **2021**, *50*, 3519.

(24) Wachs, I. E.; Roberts, C. A. Monitoring surface metal oxide catalytic active sites with Raman spectroscopy. *Chem. Soc. Rev.* **2010**, *39*, 5002.

(25) McBreen, P. H.; Moskovits, M. A surface-enhanced Raman study of ethylene and oxygen interacting with supported silver catalysts. *J. Catal.* **1987**, *103*, 188.

(26) Stiles, P. L.; Dieringer, J. A.; Shah, N. C.; Duyne, R. P. V. Surface-Enhanced Raman Spectroscopy. *Annu. Rev. Anal. Chem.* **2008**, *1*, 601.
(27) Shao, F.; Zenobi, R. Tip-enhanced Raman spectroscopy: principles, practice, and applications to nanospectroscopic imaging of 2D materials. *Anal. Bioanal. Chem.* **2019**, *411*, 37.
(28) Kurouski, D.; Dazzi, A.; Zenobi, R.; Centrone, A. Infrared and Raman chemical imaging and spectroscopy at the nanoscale. *Chem. Soc. Rev.* **2020**, *49*, 3315.
(29) Su, H.-S.; Feng, H.-S.; Zhao, Q.-Q.; Zhang, X.-G.; Sun, J.-J.; He, Y.; Huang, S.-C.; Huang, T.-X.; Zhong, J.-H.; Wu, D.-Y.; Ren, B. Probing the Local Generation and Diffusion of Active Oxygen Species on a Pd/Au Bimetallic Surface by Tip-Enhanced Raman Spectroscopy. *J. Am. Chem. Soc.* **2020**, *142*, 1341.
(30) Yin, H.; Zheng, L.-Q.; Fang, W.; Lai, Y.-H.; Porenta, N.; Goubert, G.; Zhang, H.; Su, H.-S.; Ren, B.; Richardson, J. O.; Li, J.-F.; Zenobi, R. Nanometre-scale spectroscopic visualization of catalytic sites during a hydrogenation reaction on a Pd/Au bimetallic catalyst. *Nat. Catal.* **2020**, *3*, 834.
(31) van Schrojenstein Lantman, E. M.; Deckert-Gaudig, T.; Mank, A. J. G.; Deckert, V.; Weckhuysen, B. M. Catalytic processes monitored at the nanoscale with tip-enhanced Raman spectroscopy. *Nat. Nanotechnol.* **2012**, *7*, 583.
(32) Chen, Z.; Jiang, S.; Kang, G.; Nguyen, D.; Schatz, G. C.; Van Duyne, R. P. Operando Characterization of Iron Phthalocyanine Deactivation during Oxygen Reduction Reaction Using Electrochemical Tip-Enhanced Raman Spectroscopy. *J. Am. Chem. Soc.* **2019**, *141*, 15684.
(33) Nguyen, D.; Kang, G.; Chiang, N.; Chen, X.; Seideman, T.; Hersam, M. C.; Schatz, G. C.; Van Duyne, R. P. Probing Molecular-Scale Catalytic Interactions between Oxygen and Cobalt Phthalocyanine Using Tip-Enhanced Raman Spectroscopy. *J. Am. Chem. Soc.* **2018**, *140*, 5948.
(34) Sun, M. T.; Zhang, Z. L.; Zheng, H. R.; Xu, H. X. In-situ plasmon-driven chemical reactions revealed by high vacuum tip-enhanced Raman spectroscopy. *Sci. Rep.* **2012**, *2*, 4.
(35) Xu, S.; Cruchon-Dupeyrat, S. J. N.; Garno, J. C.; Liu, G.-Y.; Jennings, G. K.; Yong, T.-H.; Laibinis, P. E. In situ studies of thiol self-assembly on gold from solution using atomic force microscopy. *J. Chem. Phys.* **1998**, *108*, 5002.
(36) Schreiber, F.; Eberhardt, A.; Leung, T. Y. B.; Schwartz, P.; Wetterer, S. M.; Lavrich, D. J.; Berman, L.; Fenter, P.; Eisenberger, P.; Scoles, G. Adsorption mechanisms, structures, and growth regimes of an archetypal self-assembling system: Decanethiol on Au(111). *Phys. Rev. B* **1998**, *57*, 12476.
(37) Zhang, Z.; Chen, L.; Sun, M.; Ruan, P.; Zheng, H.; Xu, H. Insights into the nature of plasmon-driven catalytic reactions revealed by HV-TERS. *Nanoscale* **2013**, *5*, 3249.
(38) Sun, M.; Zhang, Z.; Kim, Z. H.; Zheng, H.; Xu, H. Plasmonic Scissors for Molecular Design. *Chem.-Eur. J.* **2013**, *19*, 14958.
(39) El-Khoury, P. Z.; Aprà, E. Spatially Resolved Mapping of Three-Dimensional Molecular Orientations with ∼2 nm Spatial Resolution through Tip-Enhanced Raman Scattering. *J. Phys. Chem. C* **2020**, *124*, 17211.
(40) Zhao, L.-B.; Zhang, M.; Huang, Y.-F.; Williams, C. T.; Wu, D.-Y.; Ren, B.; Tian, Z.-Q. Theoretical Study of Plasmon-Enhanced Surface Catalytic Coupling Reactions of Aromatic Amines and Nitro Compounds. *J. Phys. Chem. L* **2014**, *5*, 1259.
(41) van Schrojenstein Lantman, E. M.; Gijzeman, O. L. J.; Mank, A. J. G.; Weckhuysen, B. M. Investigation of the Kinetics of a Surface Photocatalytic Reaction in Two Dimensions with Surface-enhanced Raman Scattering. *ChemCatChem* **2014**, *6*, 3342.

TOC: